ORIGINAL PAPER

An amperometric glucose biosensor based on electrostatic force induced layer-by-layer GOD/chitosan/pyrite on a glassy carbon electrode

Tingting Ma[1,2] · Yue Wang[1] · Ying Hou[2] · Enlei Wang[2] · Guoqing Yin[1] · Yasushi Hasebe[3] · Zhiqiang Zhang[1]

Abstract

Pyrite (PR), as a representative sulfide mineral, possesses the advantages of abundancy, thermodynamic stability, non-toxicity and semi-conductivity. In this study, an amperometric glucose biosensor (GOD/CS/PR/GCE) based on layer-by-layer of glucose oxidase (GOD), chitosan (CS) and pyrite (PR) on a glassy carbon electrode (GCE) was fabricated through electrostatic force. In this research, PR suspension prepared in phosphate buffer (pH 5.5) was first immobilized on the GCE surface, which exhibits a negative charge. Then, positively charged CS was adsorbed on the PR/GCE by electrostatic force. Finally, negatively charged GOD was further modified on the CS/PR/GCE surface through electrostatic force again. The surface morphology and adsorbance mechanism were supported by field emission scanning electron microscopy, quartz crystal microbalance with dissipation and atomic force microscope. The step-by-step procedure gives both strong adhesion ability and good bioelectrocatalytic activity of GOD on the CS- and PR-modified electrode surface. The linear range of this GOD/CS/PR/GCE biosensor was achieved from 0.5 to 60 mM with the linear regression equation of $y = 0.897x - 0.3016$ ($R^2 = 0.9996$) and a limit of detection value of 50 μM. This approach of using pyrite and chitosan as physically modified GOD to serve as electrostatic glues could be useful for designing better enzyme-based biosensors for a wide variety of practical applications.

Keywords Pyrite · Chitosan · Glucose oxidase · Glucose biosensor · Glassy carbon electrode · Layer-by-layer modification

✉ Yue Wang
  wangyue@ustl.edu.cn

✉ Zhiqiang Zhang
  zhangzhiqiang@ustl.edu.cn

1   School of Chemical Engineering, University of Science and Technology Liaoning, 185 Qianshan Middle Road, High-Tech Zone, Anshan 114051, Liaoning, China

2   School of Mineral Engineering, University of Science and Technology Liaoning, 185 Qianshan Middle Road, High-Tech Zone, Anshan 114051, Liaoning, China

3   Department of Life Science and Green Chemistry, Faculty of Engineering, Saitama Institute of Technology, 1690 Fusaiji, Fukaya, Saitama 369-0293, Japan

Introduction

Glucose plays an important role in energy replenishment, liver detoxification and memory enhancement in organisms. Abnormal blood glucose levels can result in diseases such as diabetes, cardiopathy, nephropathy, hypoglycemia, stroke or cardiovascular disorders. Diabetes is one of the biggest threats to human health globally and the number of diabetic patients increases year by year [1–3]. In addition, glucose is extensively used in various fields such as confectionery manufacturing, food processing, clinical applications and the wine industry [4, 5]. Therefore, the sensitive and accurate detection of glucose concentration is of great significance for the monitoring and treatment of related diseases and the control of industrial processes.

Compared with traditional analytical methods, for instance, spectrophotometry [6], fluorescence [7], titrimetry [8], high-performance and liquid chromatography (HPLC) [9], electrochemical biosensors have attracted great attention for their high sensitivity, excellent selectivity, low cost, eco-friendliness, and fast detection speed [10–13].

Enzymes are promising green catalysts in the field of pharmaceutical intermediates, drugs and fine chemicals due to their renewability, earth-abundant and low cost properties [14]. The many functional materials used in enzyme biosensors, include polymer [15], noble metal nanomaterials [16], grapheme [17, 18], sol–gel [19], ionic liquid [20], ceramic matrix [21, 22], and sulfide mineral [23–27]. Pyrite (PR), as the most abundant sulfide ore in the earth, with the molecular formula of FeS_2, is a Fe(II) polysulfide-based cubic NaCl-type crystalline structure. It has been used as a cathode material for thermal batteries due to its excellent properties such as suitable redox electromotive force, high thermodynamic stability, suitable conductivity, and a fixed platform that can be charged and discharged [28]. Owing to the excellent electrochemical performance and the ability to transfer heterogeneous electrons, it has been studied extensively in electrochemical catalysis and sensing [29–31].

Glucose oxidase (GOD, β-D-glucose) is a typical oxidoreductase and has been extensively applied in enzyme biosensors for the quantitative detection of glucose in both clinical diagnostics and food industry analysis [32]. It uses molecular oxygen as an electron acceptor to catalyze the oxidation of β-D-glucose to δ-gluconolactone, which then hydrolyzes into gluconic acid and hydrogen peroxide spontaneously [33]. Usually, the use of enzymes outside the biological environments has challenge limitations including high cost, sensitivity to surroundings, and narrow specificity. The methods for immobilization of GOD on electrodes include physical adsorption [34, 35], covalent bonding, cross-linking [36–38], and entrapment in gels [39–41]. Each of these immobilization methods has its own advantages and disadvantages. Among them, physical adsorption is one of the simplest methods and it has attracted considerable attention for fabricating biosensors.

Chitosan (CS, (1→4)-β-D-glucosamine) is a kind of abundant natural polymer derived from chitin and widely exists in the polysaccharides of insects, arthropods and crustaceans. CS has the advantages of low cost, high mechanical strength, chemical inertia, good hydrophilicity and strong film-forming ability. This special polymer has important applications in the field of electroanalytical chemistry due to its non-toxicity and good biocompatibility [42, 43].

In this study, an amperometric glucose biosensor was constructed through layer-by-layer (LbL) physical adsorption of pyrite, CS and GOD on a glassy carbon electrode (GCE) using electrostatic force. The LbL technique is a widely used adsorption method of alternately depositing layers of a charged protein and oppositely charged species through electrostatic interactions [44]. It is an effective approach for enzyme immobilization due to its simplicity and mild operate condition. The LbL method is suitable for immobilizing different enzyme architectures with low denaturation effects because most enzymes are water-soluble and charged in solution phase [45]. Chitosan is a cationic polymer and has been the most widely employed for electroanalytical purposes [46]. The negative-charged PR/positive-charged CS/negative-charged GOD-based structure of this biosensor is useful to keep both the bioelectrocatalytic activity and stability of adsorbed GOD due to strong electrostatic interaction. The adsorbed GOD exhibited adequate mediated response current towards glucose. In addition, the hydration layer of CS promotes the retention of the GOD structure and activity to a significant extent [47]. Chitosan and pyrite worked as suitable protein glues, which bind to both the GOD and the GCE surface. These data suggested that raw pyrite could also be used directly as glucose oxidase-based mediated electrochemical sensor after careful design.

Experimental

Reagents and materials

Glucose oxidase (GOD, EC 1.1.3.4 from *Aspergillus niger*; > 100 units/mg) was purchased from Sigma-Aldrich Co., China. Glucose, chitosan (CS), hydroquinone (HQ), ferrocene (FC), dopamine (DA), catechol (CC), KH_2PO_4 and K_2HPO_4 were obtained from Sinopharm Chemical Reagent Co., Ltd (China). A 0.1 M phosphate buffer (prepared using KH_2PO_4 and K_2HPO_4) was used to prepare the electrolyte. Ferrous disulfide (FeS_2) was obtained from Tongling Weight Mineral Products Sales Co., Ltd. Pyrite (PR) was achieved from Yichun Luming Mining Co., Ltd. (Yichun, China). Pure FeS_2 chips for QCM-D were purchased from Biolin (Shanghai) Trading Co., Ltd. All reagents were used without further purification.

Apparatus

The morphology of the modified electrode was observed by use of field emission scanning electron microscope (FE-SEM) (SIGMA-HD, ZEISS). The phase and composition of pyrite were obtained by X-ray diffraction (D8 Advance, Bruker). The fabricated process was characterized by quartz crystal microbalance (QCM-D) and atomic force microscope (AFM). Electrochemical measurements were performed with a CHI 750D workstation (Shanghai Chenhua, China). A traditional three-electrode system was used with modified pyrite electrode as working electrode, Ag/AgCl (sat. KCl) as reference electrode and Pt wire as counter electrode. All experiments were conducted at room temperature of approximately 20 °C.
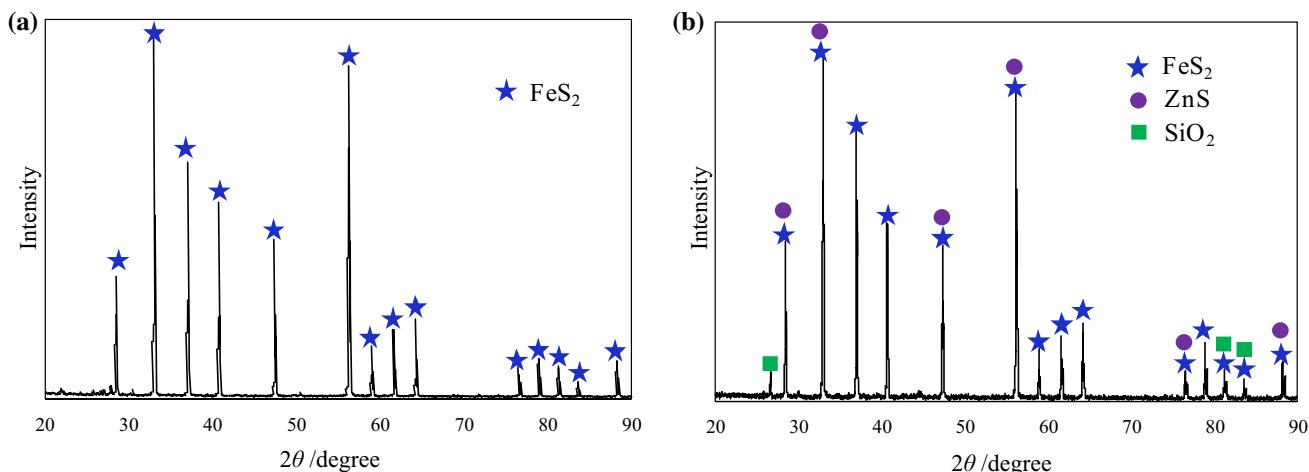
Fig. 1 Preparation of GOD/CS/PR/GCE biosensor

Fig. 2 XRD patterns of pure FeS_2 (**a**) and natural pyrite (**b**)

Preparation of the GOD/CS/PR/GCE biosensor

A glassy carbon electrode was polished with 1.0 and 0.05 µm of α-alumina slurries powder, respectively. The GCE was sonicated with deionized water to remove adhered alumina and any impurities. Then, 30 mg/mL of PR suspension (10 µL) was dropped on the cleaned GCE surface and allowed to dry in air. Next, a chitosan (0.05%) aqueous solution was dropped on the PR/GCE surface and allowed to continue to dry naturally. Finally, GOD (2 mg/mL) solution was casted on the CS/PR/GCE surface to prepare the biosensor (GOD/CS/PR/GCE). The preparation process is shown in Fig. 1.

Results and discussion

### Characterization of pyrite and pyrite-based biosensor

The phase characteristics of FeS_2 and natural pyrite were examined by X-ray diffraction (XRD) and the results are shown in Fig. 2. The composites contents were calculated and are listed in Table 1. It can be seen that the contents of FeS_2 in natural pyrite and pure FeS_2 were 78.8 and 99.5%, respectively. The main impurities of natural pyrite are ZnS and SiO_2, respectively. In addition, the cyclic voltammetry

Table 1 XRD analysis of pure FeS_2 and natural pyrite

Materials	FeS_2 (%)	Other impurities (%)
FeS_2	99.5	0.5
Pyrite	78.8	21.2

(CV) methods were used to evaluate the performances of GOD/CS/PR/GCE and GOD/CS/FeS$_2$/GCE, which were prepared in the same way. The response peak current of GOD/CS/FeS$_2$/GCE to glucose was 35% higher than that of GOD/CS/PR/GCE (data not shown). Hence, we think the purity of mineral is important to obtain a better current response.

The structures and morphologies of PR/GCE (a), GOD/PR/GCE (b), CS/PR/GCE (c), and GOD/CS/PR/GCE (d) were characterized by FE-SEM. Figure 3a shows that the raw pyrite is in a bulky shape. The edges of PR are clearly observed and the GOD layer seems thin on the PR surface in Fig. 3b. Hence, we speculated that GOD cannot cover the PR surface completely when it was directly adsorbed on the PR-modified GCE as shown in Fig. 3b. In comparison to Fig. 3b, the granular and rounded morphology are observed in Fig. 3c. This is attributed to the strong film-forming ability of chitosan. Figure 3d shows a thick and film-like layer of GOD on the CS/PR/GCE electrode surface. To verify
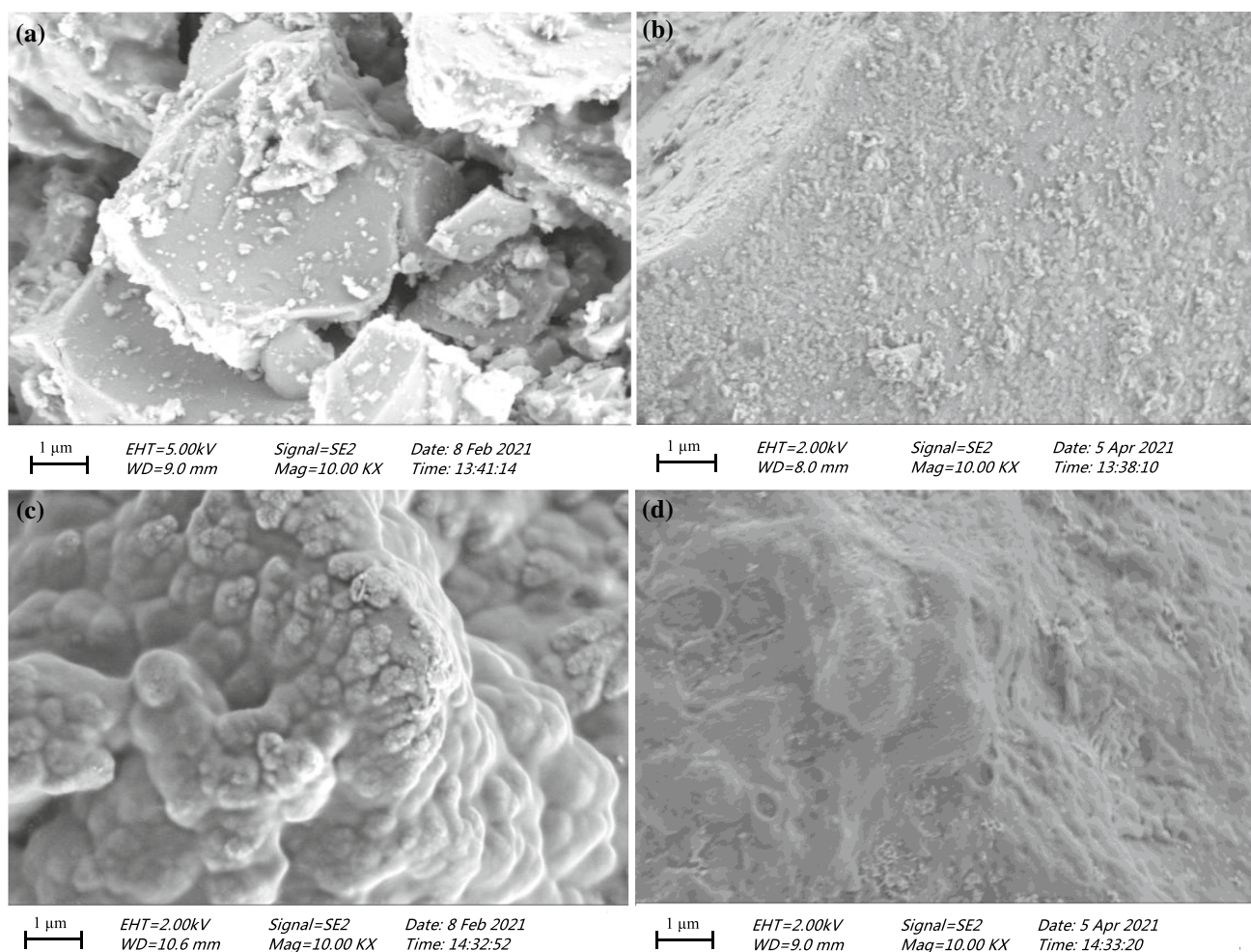
Fig. 3 The SEM images of **a** PR/GCE, **b** GOD/PR/GCE, **c** CS/PR/GCE, and **d** GOD/CS/PR/GCE

our speculation, we measured the XRD in different cases, including PR, GCE, CS, GOD, CS/GCE, PR/GCE, CS/PR/GCE, and GOD/CS/PR/GCE, respectively. Without CS modification, the sharp peaks of PR were observed clearly even on the GOD/PR/GCE surface (data not shown). However, in the presence of CS, the sharp peaks of PR were invisible. Therefore, the cationic CS is essential to tightly adsorb the negative-charged PR and GOD, which gives a stable layer-by-layer structure.

Electrochemical behaviors of the modified electrode surface

In this study, hydroquinone (HQ) was used as electron transfer mediator to evaluate the biocatalytic activity of GOD adsorbed on a chitosan-modified PR-based electrode in the presence of nitrogen. The detection mechanism of glucose in this biosensor is according to the following scheme [48, 49]:

$$\text{Hydroquinone (HQ)} \rightarrow p\text{-quinone} + 2\text{H}^+ + 2\text{e}^-, \tag{1}$$

$$\text{GOD(FAD)} + \text{D-glucose} \rightarrow \text{GOD}\left(\text{FADH}_2\right) + \text{D-glucono-}\delta\text{-lactone}, \tag{2}$$

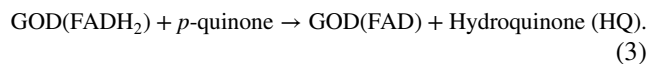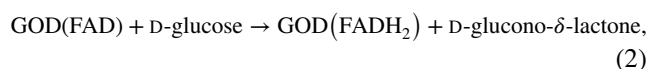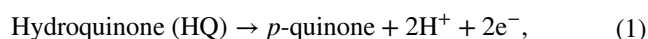$$\text{GOD(FADH}_2) + p\text{-quinone} \rightarrow \text{GOD(FAD)} + \text{Hydroquinone (HQ)}. \tag{3}$$

Figure 4 shows the CV curves with and without glucose by four different modified electrodes. The catalytic current values for the oxidation of 20 mM glucose of the GOD/CS/PR/GCE (a), GOD/CS/GCE (b), GOD/PR/GCE (c), and GOD/GCE (d) are 66.0, 47, 6.9, and 3.1 μA at the potential of 0.6 V vs Ag/AgCl, respectively. A comparison of Fig. 4c, d shows PR is useful in enhancing the biocatalytic activity of GOD on the GCE surface. From Fig. 4b, it can be observed that the catalytic current value of GOD/CS/GCE is about 6.8 times that of GOD/PR/GCE. It could be concluded that the CS has good adhesion ability and opposite charges to GOD. The best response current was obtained by GOD/CS/
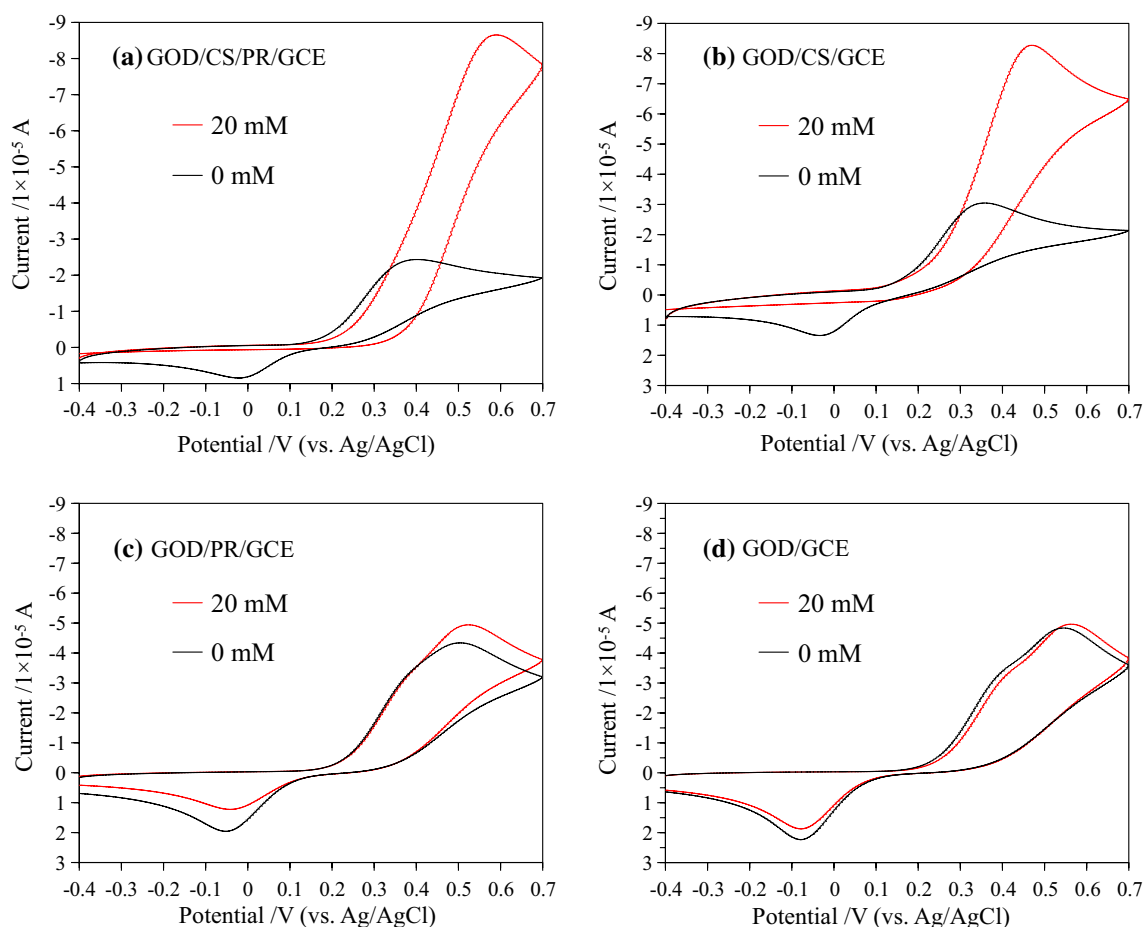
Fig. 4 Cyclic voltammograms of the GOD/CS/PR/GCE (**a**), GOD/CS/GCE (**b**), GOD/PR/GCE (**c**), and GOD/GCE (**d**) in N_2-saturated 0.1 M PBS (pH 5.5) containing 5 mM HQ with (red) and without glu-cose (black). The potential scan rate is 5 mV/s, and the starting potential is − 0.4 V vs Ag/AgCl

PR/GCE, which is 1.4 times higher than GOD/CS/GCE. We speculate the synergistic effect of CS and PR would be useful for keeping suitable orientation and enhancing the biocatalytic activity of GOD. To understand the reason of this phenomena, the following electrochemical method, QCM-D and AFM measurements were used to explain the response to glucose of adsorbed GOD on differently immobilized surfaces.

The structure and conformation of immobilized enzyme largely affect the electrocatalytic activity and electron transfer performance of enzyme-based biosensor. To obtain the electrochemical properties of the modified electrodes, we measured cyclic voltammograms (CV) of GOD/CS/PR/GCE (green), CS/PR/GCE (red), PR/GCE (blue) and bare GCE (brown) in 5 mM $[Fe(CN)_6]^{3-/4-}$ containing PBS (0.1 M, pH 5.5) at a scan rate of 100 mV/s (Fig. 5a). The potential difference (ΔE) between the oxidation peak and reduction peak of the CS/PR/GCE, GOD/CS/PR/GCE, bare GCE, and PR/GCE were 101, 171, 328.7 and 402 mV, respectively. As compared to bare GCE and PR/GCE, the CS-modified

electrodes (GOD/CS/PR/GCE, CS/PR/GCE) tend to facilitate the electron transfer rate.

EIS is an effective tool for evaluating the interface properties of the modified electrode surface. The charge transfer resistance (R_{ct}) can be quantified according to the diameter of the semicircle of the Nyquist plot, and is a useful parameter for evaluating the interface properties of the adsorbed protein layer on the electrode surface [50]. Figure 5b shows the Nyquist plots of PR/GCE (blue), bare GCE (brown), GOD/CS/PR/GCE (green) and CS/PR/GCE (red) obtained using $[Fe(CN)_6]^{3-/4-}$ as an electrochemical redox probe, respectively. The R_{ct} of the CS/PR/GCE-, GOD/CS/PR/GCE-, bare GCE-, and PR/GCE-modified electrodes were 75, 240, 570, and 700 Ω, respectively. The PR/GCE showed a larger R_{ct} value compared with the bare GCE, which is attributed to the semi-conductivity of pyrite. In addition, electrostatic repulsion between negatively charged PR and $[Fe(CN)_6]^{3-/4-}$ also may be responsible for the larger R_{ct}. Differing from the prediction, the R_{ct} of CS/PR/GCE and GOD/CS/PR/GCE were smaller than those of bare GCE

(a)

(b)
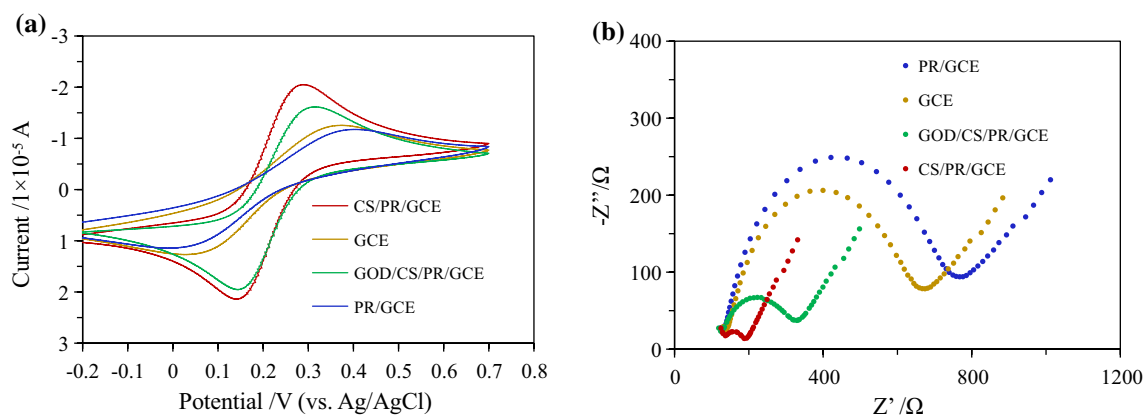
Fig. 5 CVs (**a**) and EIS (**b**) Nyquist plots of the PR/GCE (blue), bare GCE (brown), GOD/CS/PR/GCE (green) and CS/PR/GCE (red), The electrolyte is N_2-saturated 0.1 M PBS (pH 5.5) containing 5 mM $[Fe(CN)_6]^{3-/4-}$. The potential was set to the formal potential of the

$[Fe(CN)_6]^{3-/4-}$ redox system. The amplitude is 0.005 V. The frequency is from 0.1 Hz to 10 kHz. Concentrations of each species in adsorption solution: [PR] = 40 mg/mL (dispersion); [GOD] = 2 mg/mL; [CS] = 0.05% (v/v %)

and PR/GCE. At pH 5.5, CS ($pK_a \approx 10.4$) exists in cationic form [51]. Thus, it can be regarded that the electrostatic binding between the cationic CS and negatively charged $[Fe(CN)_6]^{3-/4-}$ would accelerate the electron transfer of $[Fe(CN)_6]^{3-/4-}$ or permeation of $[Fe(CN)_6]^{3-/4-}$ across the adsorbed GOD/CS/PR/GCE layer, and eventually leads to a smaller R_{ct} [52].

Optimization of experimental conditions

Since the detection process is usually affected by the dissolved oxygen, various redox active mediators (e.g., hydroquinone, hexacyanoferrate (III), *p*-benzoquinone, catechol, dopamine, and ferrocene derivatives) were used to replace molecular oxygen as the electron acceptor of GOD, which could eliminate the interference of dissolved oxygen for the second generation GOD biosensors. Here, four mediators hydroquinone (HQ), ferrocene (FC), catechol (CC), and dopamine (DA) were selected and compared in this research. As shown in Fig. 6a, the performance of HQ is the best among the selected mediators. Therefore, HQ was chosen as the mediators in subsequent experiments.

Figure 6b shows the optimization of PR concentration for the detection of 20 mM glucose by CV measurement. The response current towards glucose increases in the concentration range from 20 to 40 mg/mL and reaches a maximum value at 40 mg/mL of pyrite. Thus, 40 mg/mL was chosen as the optimal PR concentration for the following experiment. The influence of the chitosan concentration ranges from 0.02 to 0.3% (v/v%) on the peak current response was also investigated, and the results are shown in Fig. 6c. The current response of the GOD/CS/PR/GCE reaches the highest value when the concentration of chitosan is 0.05%. A certain amount of CS is essential to keep the adhesion ability

of GOD on the PR surface. However, a higher concentration of chitosan would hinder the electron transfer rate of immobilized GOD. Therefore, 0.05% of chitosan was used in the following experiments.

A series of GOD concentrations including 1.0, 1.5, 2.0, 2.5, 3.0, and 3.5 mg/mL were optimized to obtain the best electrochemical performance of GOD/CS/PR/GCE as shown in Fig. 6d. When the GOD concentration is higher than 2 mg/mL, the current response decreased severely. Therefore, 2 mg/mL glucose oxidase was selected in this experiment. The adsorption pH is important for immobilized enzymes. The effect of the adsorption pH of GOD on the CV response to glucose was also investigated over a pH range from 4.5 to 8.0 using 0.1 M PBS (Fig. 6e). The maximum current response was obtained at a pH of 5.5, which is in accordance with the optimal pH of GOD [33]. In addition, the effect of electrolyte pH showed little difference from the pH range of 4.5–6.5. And the maximum peak current value is also 5.5. At pH 5.5, PR, CS and GOD are negatively charged, positively charged and negatively charged, respectively. The three layers of PR, CS and GOD were tightly adsorbed through electrostatic force. Furthermore, maximum protein adsorption is often observed at a pH value close to p*I* of the protein, due to reduced electrostatic repulsion of neighboring proteins [53].

Adsorption behavior of GOD evaluated by quartz crystal microbalance with dissipation (QCM-D)

QCM-D is a very sensitive instrument for measuring the mass changes of adsorption species in terms of the change of resonance frequency, ΔF, and for obtaining the information of viscoelasticity in terms of the change of dissipation factor, ΔD [54, 55]. The surface mass change of quartz crystal
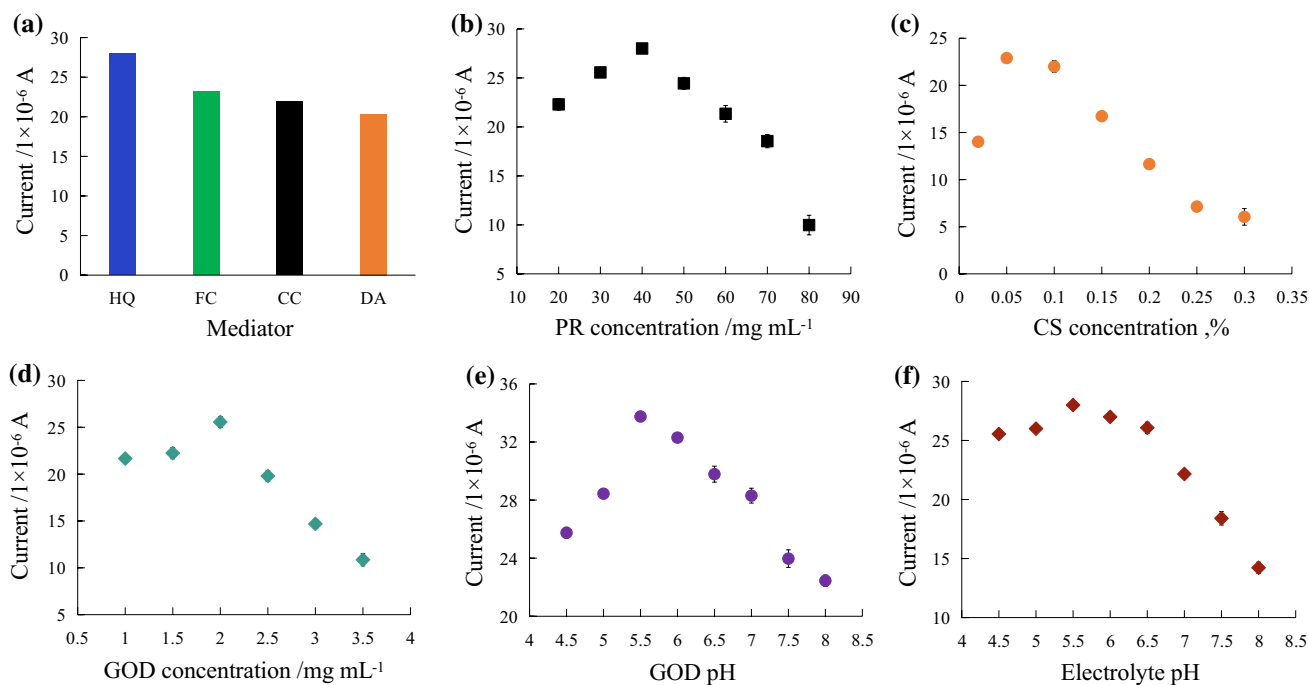
Fig. 6 Effect of mediators (**a**), PR concentration (**b**), CS concentration (%) (**c**), GOD concentration (**d**), GOD adsorption pH (**e**), and electrolyte pH (**f**) on the catalytic current response for 20 mM glucose. [PR]=40 mg/mL (for panels **a**, **c**–**f**); [CS]=0.05% (v/v %) (for panels **a**, **b**, and **d**–**f**); [GOD]=2 mg/mL (for panels **a**–**c**, **e**–**f**); electrolyte pH 5.5 (for panels **a**–**e**)

oscillator was converted to a frequency change of the output electrical signal, which is used to characterize the mass change and thickness of the adsorbed proteins. In addition, the conformational change of proteins and the hydration level of the biomolecule films could also be evaluated by QCM-D [53].

To understand the adsorption mechanisms, we studied the role of CS on the adsorption of GOD with the use of QCM-D equipped with a pure FeS$_2$ sensor tip. Figure 7a shows the QCM-D results of step-by-step adsorption of CS and GOD on the FeS$_2$ tip (GOD/CS/FeS$_2$). Figure 7b shows the adsorption of GOD alone on FeS$_2$ tip (GOD/FeS$_2$). The first
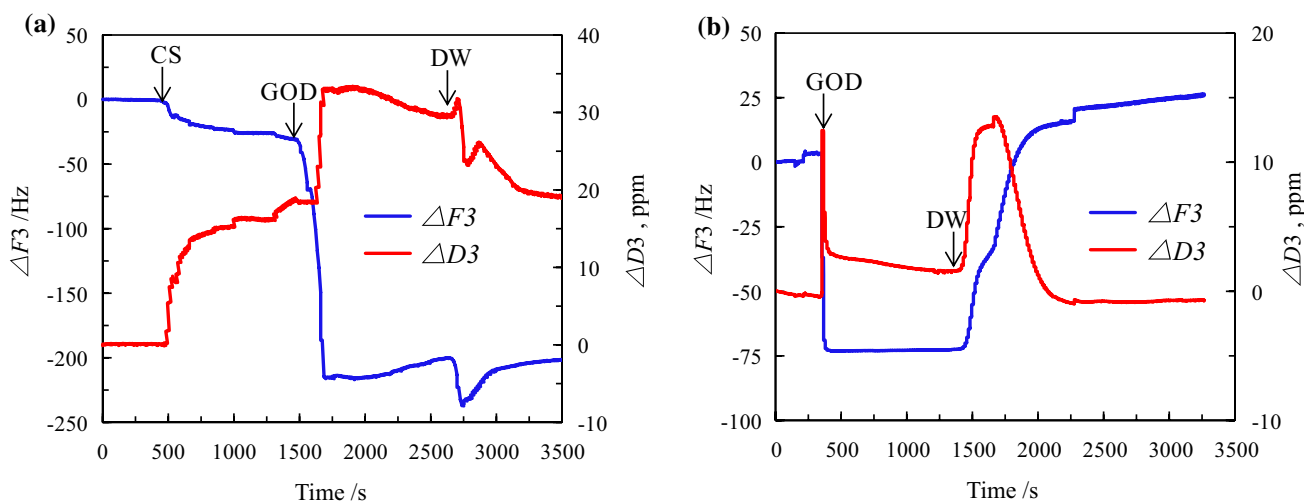
Fig. 7 QCM-D responses for the step-by-step adsorption of GOD/CS/FeS$_2$ (**a**), GOD/FeS$_2$ (**b**) on the FeS$_2$ tips in 0.1 M PBS (pH 5.5). Changes in frequency and dissipation at 15 MHz. The experiment

was conducted at 25 °C ([GOD]=2 mg/mL; [CS]=0.05%). The carrier and sample flow rate were 100 μL/min

decrease in frequency in Fig. 7a was related to the adsorption of chitosan on the FeS$_2$ sensor tip. The net ΔF gradually increased to ca. 50 Hz, which corresponds to the mass of the adsorbed CS. The frequency further decreased from -50 to -230 Hz (net ΔF, 180 Hz) when GOD was injected to the system at 1500 s, illustrating that a large amount of GOD was adsorbed on the surface of CS. The adsorbed GOD was very stable on the CS-modified FeS$_2$ tip even when distilled water (DW) was added to the detecting system, except for a temporary increase caused by the adsorption of water. In addition, the frequency decreases again due to the instability of the associated water. Figure 7b shows the net ΔF was about 75 Hz in the case of GOD adsorption alone. The adsorbed GOD amount of GOD/CS/FeS$_2$ is about 2.4 times larger than that of GOD/FeS$_2$. In addition, the adsorbed GOD is very weak, and easily detached from the FeS$_2$ sensor surface when DW was added. These results indicate that the presence of pre-adsorbed chitosan enhances the adsorbed amount of GOD.

The change of dissipation reveals the information about the viscoelasticity and morphology of the FeS$_2$ sensor and is used as a method to measure the substrate thickness, hydration state and conformation [56]. The first rapid increase in dissipation ($\Delta D \approx 19$ ppm) demonstrates that the adsorption of CS causes the thickness of the substrate. Subsequently, the continued increase of dissipation result ($\Delta D \approx 15$ ppm) was caused by the further addition of GOD. However, the final ΔD value of GOD adsorbed alone (GOD/FeS$_2$) is 0 ppm, which reflects the quick (rapid) detachment of GOD from the FeS$_2$ sensor surface. These results are in accordance with the CV data in Fig. 4. Furthermore, the $\Delta D/\Delta F$ value for the GOD/CS/FeS$_2$ layer was 82×10^{-9}. A smaller $\Delta D/\Delta F$ value for the absorbed layer suggests that CS and GOD more rigidly attached to PR (FeS$_2$) [51].

A possible explanation for this result could be assessed with the role of isoelectric point. The isoelectric point of bare PR is about pH 3 [57]. When the pH value is greater than 3, the surface of PR is negatively charged. The isoelectric point of CS is 6.3 [51]. At the pH value below 6.3, chitosan has a positive charge due to protonation of amino groups. Electrostatic effect is useful to stabilize the interaction of CS and PR in the first step. In addition, the isoelectric point of GOD is 4.2 [58]. Therefore, GOD is also negatively charged in pH 5.5, and is tightly adsorbed on the positively charged CS surface. These results predict that CS worked as a double-face glue to adhere PR and GOD. Thus, the GOD on the surface of PR is not stable due to the electrostatic repulsion effect.

AFM images with the height profiles of PR/GCE (Fig. 8a), GOD/CS/PR/GCE (Fig. 8b), and GOD/PR/GCE (Fig. 8c) were evaluated. The heights of GOD/CS/PR/GCE (106 nm) and GOD/PR/GCE (102 nm) are increased in comparison to PR/GCE (95 nm). There were little height differences among the three electrodes because of the heterogeneous property of PR and the tightly adsorbed layers of PR, CS, and GOD. The modification of GOD would cover the CS/PR/GCE surface completely as seen from the rugged, uneven and hill-like image morphology. In addition, this result is also in accordance with the SEM and XRD measurements (data not shown).

Electrochemical performances of GOD/CS/PR/GCE biosensor

The CVs of GOD/CS/PR/GCE with and without glucose in 0.1 M phosphate solution (pH 5.5) containing 5 mM HQ under the nitrogen atmosphere are shown in Fig. 9. The inset graph reflects the relativity between the glucose concentrations in the electrolyte and the catalytic currents. The catalytic current increased with an increase in the concentration of glucose, indicating the GOD/CS/PR/GCE biosensor has a good linear relationship to glucose in the range of 0.5–60 mM, with a regression equation of
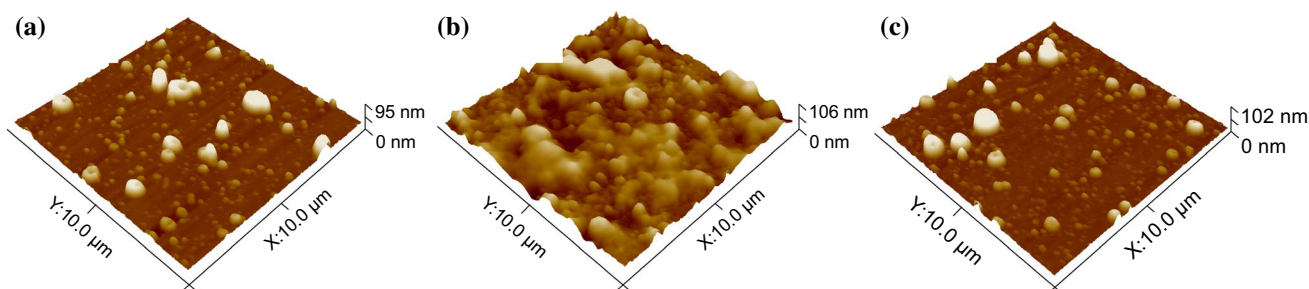
Fig. 8 AFM images of the PR/GCE (**a**), GOD/CS/PR/GCE (**b**) and GOD/PR/GCE (**c**)
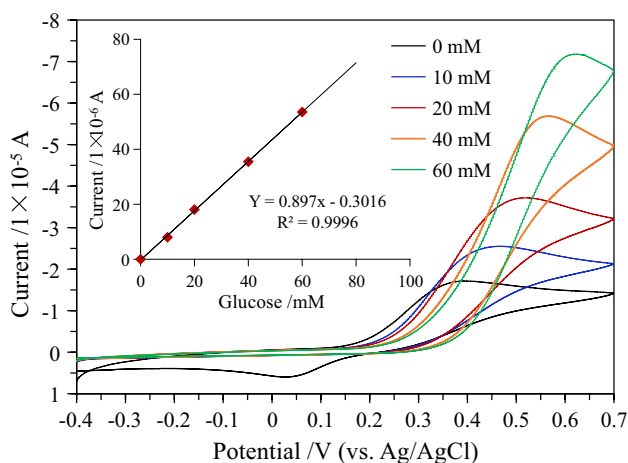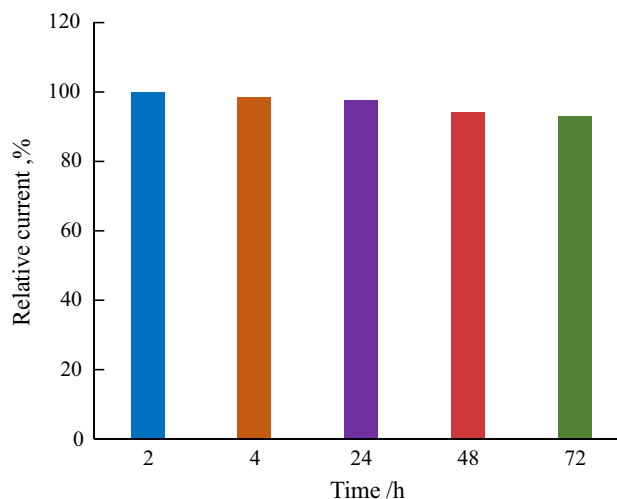
Fig. 9 CV curves of GOD/CS/PR/GCE with different concentrations of glucose in a 0.1 M phosphate solution (pH 5.5) containing 5 mM HQ in N_2 atmosphere. The potential scan rate was 5 mV/s with a starting potential of -0.4 V

Fig. 10 Long-term stability of the electrode

$I = 0.897c - 0.3016$ and a correlation coefficient of 0.9996. The detection limit (LOD) was 50 µM. Table 2 summarizes the compared characteristics of the reported GOD-based glucose biosensors. Although the LOD of this sensor is not superior with other synthesized nanomaterial-based systems, this biosensor shows an acceptable linear range, especially considering a raw mineral was used as support electrode.

Lifetime of the GOD/CS/PR/GCE biosensor

Lifetime of the same GOD/CS/PR/GCE biosensor was evaluated using the CV method towards the detection of 20 mM glucose. Figure 10 shows the peak current response which was checked at 2, 4, 24, 48, and 72 h. It was found that the biosensor lost 1.7% of the initial response at 4 h, 2.3% at 24 h, 5.8% at 48 h, and 6.9% at 72 h. This glucose biosensor was stored in a refrigerator at 4 °C in a dry state when not

in use. The results show that the electrode has good long-term stability.

Conclusions

In this study, a simple sandwich structure of GOD/CS/PR/GCE biosensor was fabricated to detect glucose through layer-by-layer electrostatic force. CS worked as a double-face glue to stabilize the GOD on the PR-modified surface. The surface morphology, adsorption mechanism, and electrochemical behaviors were examined by CV, EIS, QCM-D, SEM, and AFM instruments. If this strategy can be adopted for other sulfide minerals and enzymes, then this physical adsorption-based multilayer structure would be expected to become one of the versatile tools for developing various bioelectronic devices.

Table 2 Comparison of GOD-based electrochemical glucose biosensors

Electrode	Technique	Linear range (mM)	Detection limit (µM)	References
GOD/Pt/MOC/Au	Amperometry	0.05–3.7	50	[59]
GOD-mesoFe/C-Nafion/Pt	Amperometry	0.2–10	80	[60]
Nafion/GOD/OMC/GCE	Amperometry	0.5–15	156	[61]
GOD/AuNPs-MoS$_2$/Au	Chronoamperometry	0.25–13.2	0.042	[62]
GOD/TCT/AP/OMC/GCE	DPV	0.1–1	38	[63]
GOD/rMoS$_2$/CS/APTES/GCE	Voltammetry	3–20	–	[64]
GOD/CS/FeS$_2$/GCE	Voltammetry	0.5–60	50	This study

Pt platinum, *MOC* mesoporous carbon, *GOD* glucose oxidase, *GCE* glassy carbon electrode, *mesoFe/C* magnetic iron oxide mesoporous carbon, *rMoS$_2$* reduced MoS$_2$, *AuNPs* Au nanoparticles, *TCT* 2,4,6-trichloro-1,3,5-triazine, *AP* aminophenyl, *APTES* 3-aminopropyltriethoxysilane

Declarations

Conflict of interest On behalf of all the authors, the corresponding author states that there is no conflict of interest.

References

1. A. Samphao, P. Butmee, J. Jitcharoen, Ľ. Švorc, G. Raber, K. Kalcher, Talanta **42**, 35 (2015)
2. N.H. Cho, J.E. Shaw, S. Karuranga, Y. Huang, J.D. Rocha Fernandes, A.W. Ohlrogge, B. Malanda, Diabetes Res. Clin. Pract. **138**, 271 (2018)
3. N.I. Chandrasekaran, M. Manickam, Sens. Actuators. B **288**, 188 (2019)
4. E.B. Bahadir, M.K. Sezginturk, Anal. Biochem. **478**, 107 (2015)
5. X.H. Yuan, J.H. Wang, K. Xia, Adv. Funct. Mater. **15**, 803 (2005)
6. M.R.H. Nezhad, J. Tashkhourian, J. Khodaveisi, J. Iran. Chem. Soc. **7**, S83 (2010)
7. L. Li, X. Cai, Y. Ding, S. Gu, Q. Zhang, Anal. Methods **5**, 6748 (2013)
8. N.V. Klassen, D. Marchington, C.E. McGowan, Anal. Chem. **66**, 2921 (1994)
9. N. Li, J.Z. Guo, B. Liu, H. Cui, L.Q. Mao, Y.Q. Lin, Anal. Chim. Acta **645**, 48 (2009)
10. W. Cai, T. Lai, H. Du, J. Ye, Sens. Actuators B **193**, 492 (2014)
11. M. Ahn, J. Kim, J. Electroanal. Chem. **683**, 75 (2012)
12. D.P. Li, X.Y. Liu, R. Yi, J.X. Zhang, Z.Q. Su, G. Wei, Inorg. Chem. Front. **5**, 112 (2018)
13. S. Su, H.F. Sun, F. Xu, L.H. Yuwen, L. Wang, Electroanalysis **25**, 2523 (2013)
14. I.K. Deshapriya, C.V. Kumar, Langmuir **29**, 4001 (2013)
15. D. Ragupathy, A.I.G.K.P. Lee, Microchim. Acta **166**, 303 (2009)
16. R.S. Dey, C.R. Raj, J. Phys. Chem. C **114**, 21427 (2010)
17. B.B.G. Choi, H. Park, T.J. Park, M.H. Yang, J.S. Kim, S.Y. Jang, N.S. Heo, S.Y. Lee, J. Kong, W.H. Hong, ACS Nano **4**, 2910 (2010)
18. C. Shan, H. Yang, J. Song, D. Han, A. Ivaska, L. Niu, Anal. Chem. **81**, 2378 (2009)
19. F. Doroftei, T. Pinteala, A. Arvinte, Microchim. Acta **181**, 111 (2013)
20. V.S. Joshi, J. Kreth, D. Koley, Anal. Chem. **89**, 7709 (2017)
21. K. Thenmozhi, S. Sriman Narayanan, Anal. Bioanal. Chem. **387**, 1075 (2006)
22. D.R. Shankaran, N. Uehera, T. Kato, Anal. Bioanal. Chem. **374**, 412 (2002)
23. R. Zhao, Y. Wang, Z. Zhang, Y. Hasebe, D. Tao, Anal. Sci. **35**, 733 (2019)
24. R. Zhao, Y. Wang, Int. J. Electrochem. Sci. **15**, 1595 (2020)
25. N. Rohaizad, C.C. Mayorga-Martinez, Z. Sofer, M. Pumera, A.C.S. Appl, Mater. Interfaces **9**, 40697 (2017)
26. X. Cao, Microchim. Acta **181**, 133 (2014)
27. H. Huang, J. Zhang, M. Cheng, K. Liu, X. Wang, Microchim. Acta **184**, 4803 (2017)
28. R.A. Guidotti, P.J. Masset, J. Power, Sources **183**, 388 (2008)
29. Y. Huai, C. Plackowski, Y. Peng, Miner. Eng. **111**, 131 (2017)
30. A.P. Chandra, A.R. Gerson, Surf. Sci. Rep. **65**, 293 (2010)
31. Y. Wang, K.J. Zhao, D.P. Tao, F.G. Zhai, H.B. Yang, Z.Q. Zhang, RSC Adv. **8**, 5013 (2018)
32. X.C. Tan, Y.X. Tian, P.X. Cai, X.Y. Zou, Anal. Bioanal. Chem. **381**, 500 (2005)
33. Y. Wang, Y. Hasebe, J. Electrochem. Soc. **159**, F110 (2012)
34. M.A. Arnold, G.A. Rechnitz, Anal. Chem. **54**, 2315 (1982)
35. Y. Ikariyama, S. Yamauchi, T. Yukiashi, H. Ushioda, Anal. Lett. **20**, 1791 (1987)
36. T. Yao, Anal. Chim. Acta **148**, 27 (1983)
37. G.J. Moody, G.S. Sanghera, J.D.R. Thomas, Analyst **111**, 605 (1986)
38. B.F.Y. Yon Hin, C.R. Lowe, Anal. Chem. **59**, 2111 (1987)
39. J.X. Jing, Y.C. Hong, Anal. Biochem. **280**, 221 (2000)
40. N.C. Foulds, C.R. Lowe, J. Chem. Soc. Faraday Trans. 1 **82**, 1259 (1986)
41. J. Okuda, J. Wakai, N. Yuhashi, K. Sode, Biosens. Bioelectron. **18**, 699 (2003)
42. Y. Fang, R. Zhang, B. Duan, M. Liu, A. Lu, L. Zhang, ACS Sustain. Chem. Eng. **5**, 2725 (2017)
43. K. Zhu, J. Duan, J. Guo, S. Wu, A. Lu, L. Zhang, Biomacromol **18**, 3904 (2017)
44. G. Decher, Science **277**, 1232 (1997)
45. K. Ariga, M. Onda, Y. Lvov, T. Kunitake, Chem. Lett. **26**, 25 (1997)
46. Q. Xu, S.X. Gu, L. Jin, Y.E. Zhou, Z. Yang, W. Wang, X. Hu, Sens. Actuators B **190**, 562 (2014)
47. C.V. Kumar, A. Chaudhari, J. Am. Chem. Soc. **122**, 830 (2000)
48. Y. Wang, Y. Hasebe, J. Electrochem. Soc. **159**, F110 (2012)
49. R. Zhao, Y. Wang, Y. Hasebe, Z. Zhang, D. Tao, Int. J. Electrochem. Sci. **15**, 1595 (2020)
50. Q. Chi, J. Zhang, J.U. Nielsen, E.P. Friis, I. Chorkendorff, G.W. Canters, J.E.T. Andersen, J. Ulstrup, J. Am. Chem. Soc. **122**, 4047 (2000)
51. P. Sorlier, A. Denuzière, C. Viton, A. Domard, Biomacromol **2**, 765 (2001)
52. Y. Zhang, Y. Wang, Z. Zhang, A. Sobhy, S. Sato, M. Uchida, Y. Hasebe, ACS Omega **21**, 13719 (2021)
53. A.G. Hemmersam, K. Rechendorff, F. Besenbacher, B. Kasemo, D.S. Sutherland, J. Phys. Chem. C. **112**, 4180 (2008)
54. G. Hu, J.A. Heitmann Jr., O.J. Rojas, J. Phys. Chem. B **113**, 14761 (2009)
55. S.A. Maurer, C.N. Bedbrook, C.J. Radke, Langmuir **28**, 14598 (2012)
56. A. Kumagai, S.H. Lee, T. Endo, Biomacromol **14**, 2420 (2013)
57. W. Zhang, W. Sun, Y. Hu, J. Cao, Z. Gao, Minerals **9**, 549 (2019)
58. B.E. Swoboda, V. Massey, J. Biol. Chem. **240**, 2209 (1965)
59. X. Jiang, Y. Wu, X. Mao, X. Cui, L. Zhu, Sens. Actuators B **153**, 158 (2011)
60. J. Yu, J. Tu, F. Zhao, B. Zeng, J. Solid State Electrochem. **14**, 1595 (2010)
61. M. Zhou, L. Shang, B. Li, L. Huang, S. Dong, Biosens. Bioelectron. **24**, 442 (2008)
62. O. Parlak, A. İncel, L. Uzun, A.P.F. Turner, A. Tiwari, Biosens. Bioelectron. **89**, 545 (2017)
63. E. Ghasemi, E. Shams, N. Farzin Nejad, J. Electroanal. Chem. **752**, 60 (2015)
64. S. Wu, Z. Zeng, Q. He, Z. Wang, S.J. Wang, Y. Du, Z. Yin, X. Sun, W. Chen, H. Zhang, Small **8**, 2264 (2012)